PNAS RESEARCH ARTICLE | ENGINEERING

Type III and IV deformation twins in minerals and metals

John P. Hirth[a,2,1], Greg Hirth[b], and Jian Wang[c,2]

Contributed by John P. Hirth; received October 5, 2021; accepted February 15, 2022; reviewed by Tariq Khraishi and Hans-Rudolf Wenk

Type IV twins are defined and shown to exist in triclinic crystal systems, as well as in some monoclinic and trigonal systems. Here, we focus on Pericline twins in triclinic plagioclase as an example. Type IV twins are associated with the irrationality of one of the twinning elements that is rational for a type II twin. The formation of type IV twins is accomplished through the shear on a K_2 plane produced by the motion of twinning disconnections on a K_1 plane, followed by rotational partitioning. The same systems where type IV twins are present also have type III twins instead of type I. Without using the correct type IV analysis, one would deduce the wrong magnitude and direction of shear associated with the twinning process, the magnitude of which would increase with greater triclinicity. Types I and II twins form if and only if there are rational lattice translation vectors lying in the plane of distortion/shear. Otherwise, the twins are types III and IV.

twinning | disconnection | mineral | metal

Significance

Historically, two types of twins (I and II) have been categorized for twinning in minerals and metals. When analyzed by the topological model, a crystallographic construction used to define the defect structure of interfaces, triclinic and some other low-symmetry crystals do not fall into either category and instead form two new twinning types, namely, III and IV. Aside from accurately describing twin structures, these concepts are important for understanding the deformation of minerals such as plagioclase and for deriving constitutive models for the deformation.

Deformation (or mechanical) twins were first found by Mügge in 1883 (1). Such twins are common in many minerals with low symmetry (2–5) because the Burgers vectors for deformation twinning are small. In comparison, the Burgers vectors for glide dislocations in minerals are large owing to their large unit cells. Consequently, their line energies are large, making them difficult to form at low homologous temperatures. Because the Burgers vectors for twinning in these minerals are typically much smaller, the twinning defects have lower line energies. Thus, deformation in minerals by slip alone only occurs at high temperatures. At lower temperatures, the von Mises strain compatibility requirement is satisfied only when deformation twinning is present, with some slip as an accommodation mechanism. Similar twins can also occur as growth twins, e.g., ref. 6, which form by different mechanisms and are not considered further here.

In earlier work, we analyzed deformation twins in plagioclase (7–9). As plagioclase is a dominant phase in the crust of the Earth, Moon, Venus, and Mars, work in this area could improve our understanding of the strength and deformation mechanisms in the lithospheres of all these planetary bodies—especially for lower crustal conditions where plagioclase likely controls rheology, e.g., ref. 10. Examples of twins in plagioclase formed during deformation in the Earth's oceanic crust are shown in Fig. 1. We studied these samples owing to their relatively simple deformation history in the Earth's crust and subsequent rapid cooling rate, which inhibited exsolution and preserved the pertinent microstructure (11).

In analyzing the details of the twin interfaces, we realized that the classical definitions of pericline twins were incorrect, and thus, new definitions were needed. Descriptions of twins are characterized by twin types, which are related to the crystallographic twinning elements, namely, the twin planes and directions that characterize the twinning shear. Within a given structure, multiple twin types can arise because of the details of the nucleation and mobility of the pertinent interface defects (7, 12–14). Type I twins (2–5) have low-index mirror planes, on which twinning defects nucleate and traverse, propagating the twin. Type II twins occur when nucleation is rapid in comparison to the lateral mobility of the twinning defect; type II twins were defined (2, 3) as having a rational glide plane for the defects, which is inclined to an irrational twin plane. Historically, the notations for twinning elements include K_1 and K_2 for planes and $\boldsymbol{\eta}_1$ and $\boldsymbol{\eta}_2$ for directions, as in refs. 12 and 16–21. Instead, we use a modified Frank notation (17) for the twinning elements, namely, $k_1 = K_1$, $k_2 = K_2$, $\boldsymbol{\chi}_1 = \boldsymbol{\eta}_1$, and $\boldsymbol{\chi}_2 = \boldsymbol{\eta}_2$, for type I twins and $k_1 = K_2$, $k_2 = K_1$, $\boldsymbol{\chi}_1 = \boldsymbol{\eta}_2$, and $\boldsymbol{\chi}_2 = \boldsymbol{\eta}_1$ for type II twins. This notation is useful for characterizing defects mechanistically since k_1 is always the glide plane, but one must recall that k_1 corresponds to different classical planes, K_1 for type I and K_2 for type II. The slight modification from ref. 17 is that we use k and $\boldsymbol{\chi}$ instead of k and $\boldsymbol{\gamma}$ because there are already several other uses for $\boldsymbol{\gamma}$ in the theory.

At the time, we referred to the Albite twins as type I and the Pericline twins as type II. However, here we illustrate that, while formed by a mechanism like that for type II, Pericline twins differ in that the twinning direction is irrational. We call these type IV

Author affiliations: [a]Private address, Green Valley, AZ 54614; [b]Department of Geological Sciences, Brown University, Providence, RI 02912; and [c]Department of Mechanical and Materials Engineering, University of Nebraska–Lincoln, Lincoln, NE 68588

Author contributions: J.P.H. designed research; G.H. and J.W. performed research; J.W. analyzed data; and J.P.H. and J.W. wrote the paper.

Reviewers: T.K., University of New Mexico; and H.-R.W., University of California Berkeley.

The authors declare no competing interest.

[1]Retired.

[2]To whom correspondence may be addressed. Email: johnhirth5@gmail.com or jianwang@unl.edu.

This article contains supporting information online at http://www.pnas.org/lookup/suppl/doi:10.1073/pnas.2118253119/-/DCSupplemental.

Published March 24, 2022.

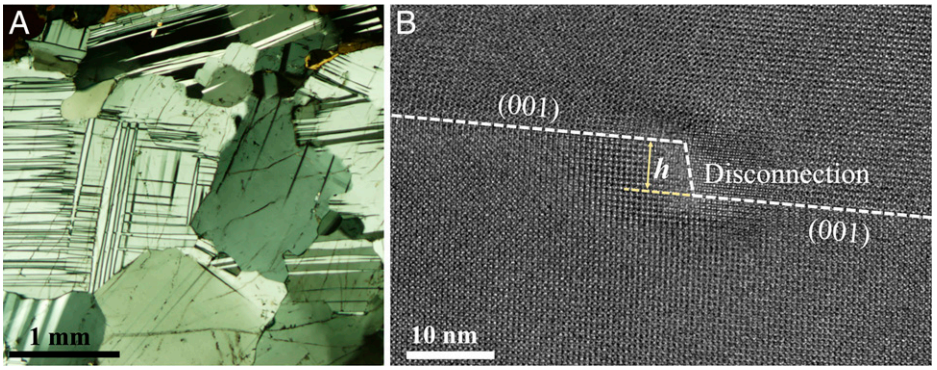

Fig. 1. (*A*). Cross-polarized light micrograph of deformed labradorite showing Albite and Pericline deformation twins. (*B*). An HRTEM image of a Pericline twin boundary containing a big step (9).

twins and define type III as the analog of type I with an irrational. The key reason for the presence of type III/IV twins in the plagioclase is the triclinic crystal structure. Such twins could also form in higher symmetry crystal structures, although there are often higher symmetry type I and type II alternatives in those materials.

Type II twins were found to form by the glide of twinning disconnections (TDs) moving on planes conjugate to the eventual type II twinning plane (15, 18, 19). Here, we apply a similar topological model (TM) model to the type IV twin for which the TD glide plane is the only rational twinning element. We determine the twinning elements for type IV twins in plagioclase and show that they differ from generally accepted values for Pericline twins. To generalize this observation, we first summarize the TM model for type I, extend the analysis to type III, and then consider type II and IV twins. The difference between type I and type III mainly entails the orientation of $\boldsymbol{\chi}_1$. However, these types also act as precursors to type II and IV, where there are major differences. Hence, we first treat the types I and II in detail and then develop the model for types III and IV.

The Physical Basis for Types I and III Twinning

The classical model for type I twinning (20–22) is illustrated in Fig. 2*A*, in which a simple (engineering) shear e is imposed on the shear plane k_1, with a displacement $\boldsymbol{u}$ in the $\boldsymbol{\chi}_1$ direction. Classically, as described in ref. 11, the shear is imposed on a unit cube and the displacement is called the shear $\boldsymbol{s}$, but this is counter to mechanics usage and the more general simple shear $\boldsymbol{e}$ is the gradient of $\boldsymbol{u}$. We prefer to use $\boldsymbol{u}$, consistent with the TM. The classical model correctly yields the TD Burgers vector $b = \boldsymbol{u}$, step height h, $\boldsymbol{e} = b/h$, and the shear angle γ_c. In the TM, the focus is instead on the symmetrical tilt-like displacements represented in Fig. 2*B*, with the characteristic angle pair 2α. These quantities are all related to twinning elements in the historical, classical-type representation in Fig. 2*C*. In the linearized classical model, the angle γ_c is set equal to the symmetric angle pair $2\alpha'$, but Fig. 2*C* shows that this is exact only in the limit that γ_c approaches zero (17, 23). Also, to nonlinear order, the angle α' in Fig. 2*C* differs from the symmetrically partitioned value α (23) since the states of strain differ. The two angles would be equal only when $\varepsilon_{xy} = (\varepsilon_{xx} - \varepsilon_{yy})/2$, and this is only true for infinitesimal strains. In other words, the distortion field of the symmetric Fig. 2*E* is equivalent to that of Fig. 2*A* plus a rotation, and these are identical only in the infinitesimal limit.

To avoid these nonlinear discrepancies, the strain is best envisioned in the hypothetical reversible cycle in Fig. 2 *B* and *D*, which emphasize the equipartitioning of the displacements. In Fig. 2*D*, the matrix M and the twin T are sheared separately by $\boldsymbol{u}_M$ and $\boldsymbol{u}_T$ as shown, and there are two differently rotated translation vectors $\boldsymbol{t}_M$ and $\boldsymbol{t}_T$ in the matrix and twin. In the TM, this process defines a type I twin. Fig. 2*E* shows the symmetrical, exact TM (3–5, 7) equivalent of Fig. 2*C*. An initial perfect reference crystal has a translation vector $\boldsymbol{t}_0$. This is displaced separately to $\boldsymbol{t}_M$ and $\boldsymbol{t}_T$ by the angle $\pm\alpha$. All displacements are in the plane of distortion. Classically, this plane was called the plane of shear, but plane of distortion is more appropriate here since both distortion components, shears and rotations, are important in the TM.

In the TM, the lattice vectors $\boldsymbol{t}_M$ and $\boldsymbol{t}_T$ are rational and low index. This requires that the origin o is a coincident lattice site. We demonstrate subsequently that in low symmetry crystals such as triclinic ones, there are no matrix translation vectors in the plane of distortion. Instead, in Fig. 2*F*, only the projections $\boldsymbol{t}_{Mp}$ and $\boldsymbol{t}_{Tp}$ of the translation vectors, with a noncoincident site origin o′, define the twin and differentiate a type III twin from a type I twin. We restrict the analysis to deformation twins, although some of the concepts apply to growth or annealing twins. The type III twinning elements are consistent with the general theoretical analysis and classification of possible types of twins (21, 22).

If the lattices of the matrix and twin in the symmetrical are superposed, the result is consistent with the TM. Fig. 2*D* shows that the distortion is partitioned equally to the top and bottom of the origin as in Fig. 2*B*. In summary, in the TM case, the displacements, Burgers vectors, and twinning angle α are all partitioned symmetrically. As discussed in ref. 23, the symmetrical TM agrees with the linearized classical model (18) only in the limit that $\alpha \to 0$. Of course, in the limit that $\alpha = 0$, there is no twin.

The Topological Models for Type I/III Twinning

The Structure of Type I/III Twins. Physically, a type I twin is propagated by gliding of TDs on k_1, and the fundamental need is to define the TD characteristics. For type I twins, the reference state in the TM (12–15) is a dichromatic pattern (DP), the superposition of twin and matrix lattices with a coincident lattice point at the origin, lying in the (commensurate) dividing surface. The characteristic parameters of a TD are defined in a DP as illustrated in the schematic Fig. 3*A*. The superposition of atoms is the dichromatic complex, which is important in considering the shuffles that complete a transformation. These are important in kinetics (7, 24), which is not considered here, so we deal only with the DP. The characteristic parameters of a TD are defined in a DP as illustrated in the schematic Fig. 3*A*. The glide plane normal unit vector P points toward the twin, a

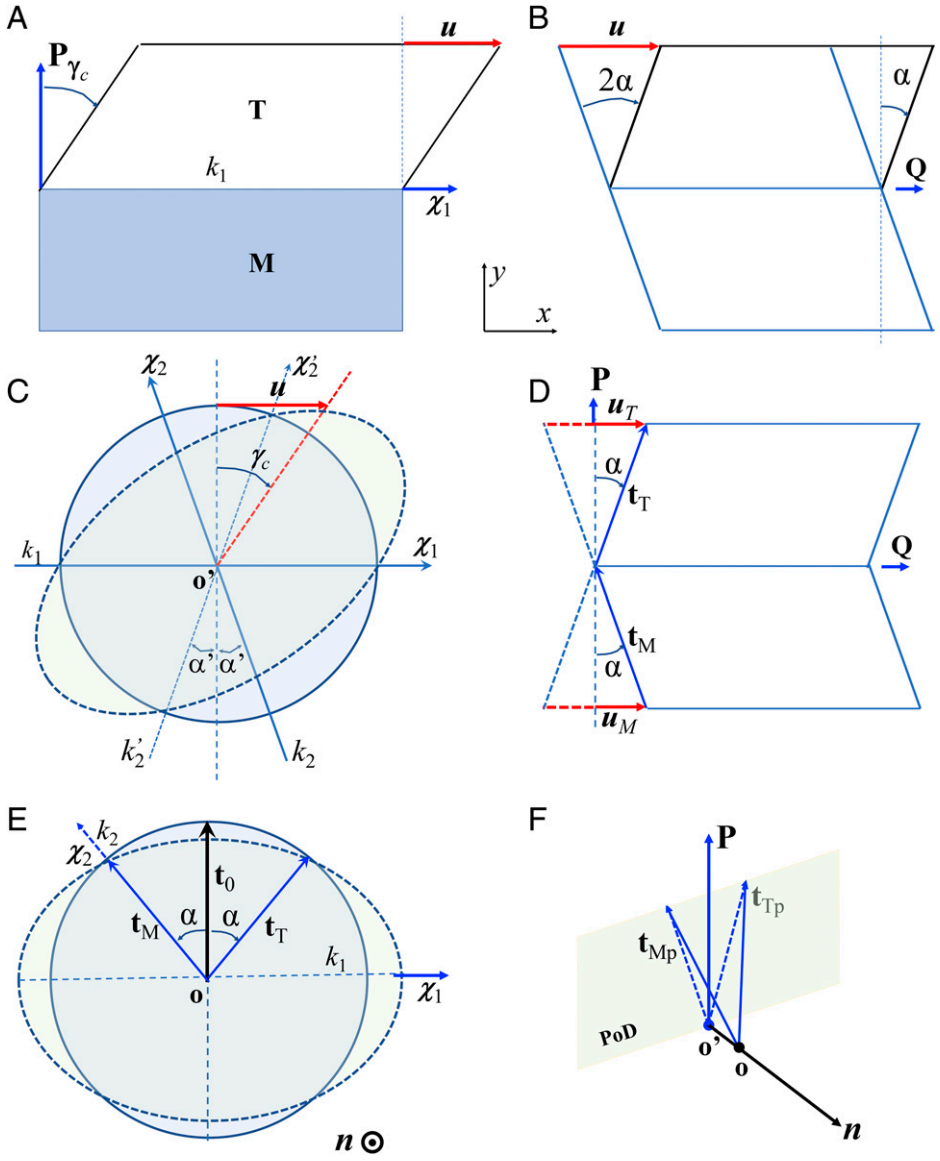

Fig. 2. (*A*) Engineering shear *e* on the k_1 plane. M is the matrix, T is the twin, and *P* is a unit vector normal to the glide plane k_1. (*B*) A symmetrically displaced parallelepiped with partitioned shear angle pairs α. (*C*) TM shear. Classical twinning elements for a circle sheared to an ellipse by the displacement $\boldsymbol{u}$. (*D*) Crystal version of *B* with translation vectors $\boldsymbol{t}_M$ and $\boldsymbol{t}_T$ and partitioned displacements $\boldsymbol{u}_M$ and $\boldsymbol{u}_T$. (*E*) Symmetrical deformation showing twinning elements. (*F*) Type III twins with a noncoincident site origin o'. PoD means the plane of distortion and *n* is its normal.

unit vector Q is parallel to the glide direction, and there is a unit vector normal to the plane of distortion, $\boldsymbol{n} = \boldsymbol{Q} \times \boldsymbol{P}$. Here, the matrix and product of the TM are expressed as M and T, respectively. The sign of the TD sense vector $\boldsymbol{\xi}$ (unit vector parallel to the disconnection line) is arbitrary, but here, we select it always to point out of the page. The TD Burgers vector is given by

$$\boldsymbol{b} = \boldsymbol{t}_T - \boldsymbol{t}_M, \qquad [1]$$

where $\boldsymbol{t}_M$ is a lattice vector in the matrix and $\boldsymbol{t}_T$ is the equivalent in the twin, expressed in matrix coordinates (Fig. 3*A*). A more complete description of the basis for Eq. **1** is presented in *SI Appendix, Matrix description of the twin in the TM*. The disconnection step height h is given by

$$h = jh_0, \qquad [2]$$

where j is an integer and h_0 is the interplanar spacing parallel to the dividing surface. A view, parallel to n, of part of a DP from an atomistic simulation for the specific case of $(10\bar{1}2)$ twins in hexagonal close packed structure, is shown in Fig. 3*B* where the shear angle is 3.8 degrees and the magnitude of Burgers vector is 0.493 Angstrom for Mg (15). The paired set 1 of t vectors for the symmetric case are $\boldsymbol{t}_M = [10\bar{1}1]_M$ and $\boldsymbol{t}_T = [10\bar{1}1]_T$, illustrated with solid lines in Fig. 3*B*, yielding Burgers vector $2\boldsymbol{b}_g$ (the subscript denotes the glide plane of the TD). An atomistic simulation of the unit TD with Burgers vector $\boldsymbol{b}_g$ is depicted in Fig. 3*C*. In principle, any paired set can be selected; an example is the set 2 shown by dashed lines, e.g., $\boldsymbol{t}_M = [10\bar{1}0]_M$ and $\boldsymbol{t}_T = [0001]_T$. For the TM twin case, to reveal crystal symmetry and the partitioning of displacements to the matrix and twin, one must select a commensurate origin such that there is a symmetric pair of t vectors like set 1, which can include a multiple step height as selected in several examples (3, 18). Fig. 3*C* has $h = 2h_o$ and, therefore, a TD Burgers vector $2\boldsymbol{b}_g$. The unit TD Burgers vector $\boldsymbol{b}_g$ (that related to displacements $\boldsymbol{u}_M$ and $\boldsymbol{u}_T$ in Fig. 3*D*) is then half the symmetric value. Only set 1 relates to Fig. 2*E* and directly gives $\boldsymbol{t}_M$ and χ_2. The use of asymmetric t vectors entails the awkward

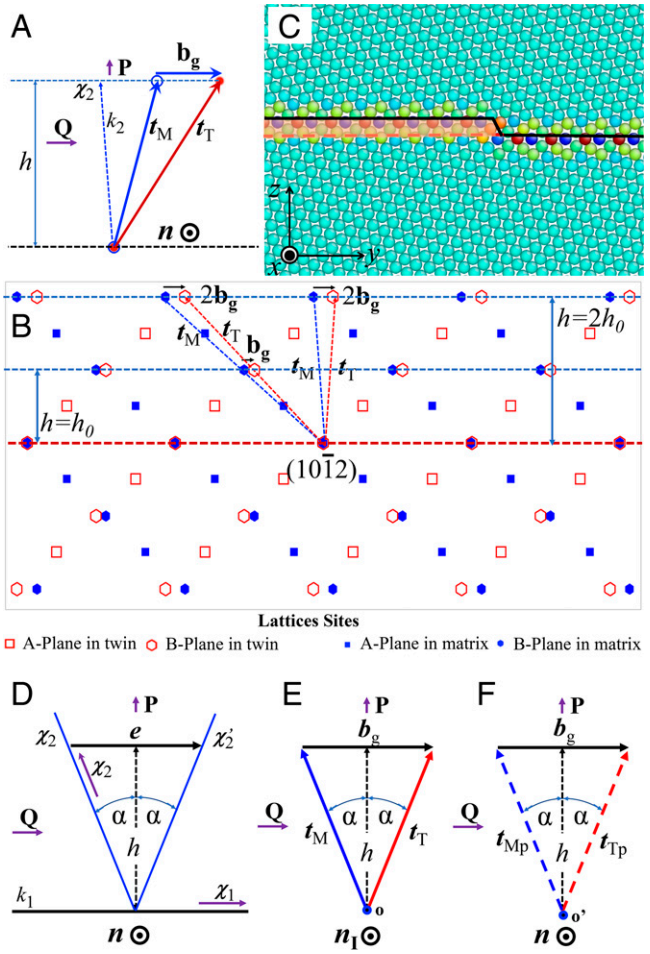

Fig. 3. (*A*) Portion of a generic DP with *t* vectors connecting lattice sites in the matrix and twin, showing the characteristics of a TD. (*B*) Portion of a DP showing the characteristics of a TD and atomic shuffles associated with a $\{10\bar{1}2\}$ twin in a hexagonal close packed structure. Two sets of possible *t* vectors (solid and dashed arrows) are shown for this type I twin. (*C*) View of the disconnection in an atomistic model of the crystal. The solid black line outlines the twin boundary. (*D*) Minimal version of the defining triangle in Fig. 2*B*, showing the twinning elements for the type I case. (*E*) Equivalent of *D* showing the TM characteristics for the type I case. (*F*) Equivalent of *D* showing the TM characteristics for the type III case.

irrational origin, greatly complicating the analysis. In some cases, asymmetric *t* vectors lead to fault formation and exchanges between nonequivalent atomic sites (7, 24). As demonstrated in refs. 9 and 14) and as employed in refs. 18 and 19, for example, in order to display partitioning of displacements to the symmetrical twin state, one must split the DP into two symmetrical DPs, so that $\boldsymbol{b}_g = (\boldsymbol{t}_0 - \boldsymbol{t}_M) + (\boldsymbol{t}_T - \boldsymbol{t}_0)$, with $\boldsymbol{t}_0$ the singe crystal reference vector in Fig. 2*E*. The DPs presented here all have this symmetrical form.

The commensurate arrangement of the twin may not yield a minimum energy interface, which could entail a rigid shift of the twin, parallel to the twin plane, by the vector *p* (8, 13, 25). This can be represented on a shifted DP (SDP) (9) that is useful in envisioning the twin and is crucial in describing shuffles. However, in determining the TD characteristics, shuffle analysis is not necessary, and it is simpler to use the symmetrical DP and then shift the symmetrical version of the twin itself by *p*. Since values of *p* are rarely known, we consider only the $p = 0$ case.

The twinning elements for type I twins corresponding to Fig. 3*B* are shown in a portion of the DP in Fig. 3*D*, and the mechanistic TM version is shown in Fig. 3*E*, including the translation vectors $\boldsymbol{t}_M$ and $\boldsymbol{t}_T$, the TD Burgers vector $\boldsymbol{b}_g$, and the TD step height *h*. The twin shear direction $\boldsymbol{\chi}_1$ is parallel to $\boldsymbol{b}_g = \boldsymbol{t}_T - \boldsymbol{t}_M$ according to Eq. **1**; and the normal to the plane of shear, *n*, is equal to $\boldsymbol{Q} \times \boldsymbol{P}$. For type I twins, $\boldsymbol{t}_M$ lies in the plane k_2 and is parallel to $\boldsymbol{\chi}_2$, so that $\boldsymbol{\chi}_2$ is rational, as in Fig. 4*A*, consistent with the classical description. For type III, Fig. 3*F*, the description is similar, but the Burgers vector is given by the projections of the irrational, dashed, *t* vectors in the plane of distortion, $\boldsymbol{b}_g = \boldsymbol{t}_{Tp} - \boldsymbol{t}_{Mp}$.

In the analysis of twinning in triclinic crystals, dating back to the work of Mügge (25), the focus is on the twin plane k_2, but the implication is that that the twinning elements are those of the classical type I twin (5, 26, 27) and, therefore, that $\boldsymbol{\chi}_1$ is rational (e.g., figure 8 in ref. 18). However, there are no twins in triclinic crystals that exhibit this topology. From a mechanistic viewpoint, the shear direction is determined kinetically by a minimum activation energy saddle point, e.g., by the direction of Peierls valleys, and may or may not be rational. For twins in plagioclase, for example, all compositions except labradorite, which is effectively monoclinic, have a twinning direction $\boldsymbol{\chi}_1$ that deviates significantly from the rational type I orientation. The type I mechanism is most easily represented in the hypothetical model in Fig. 2, where the matrix and twin are deformed separately and then joined. As shown below, this makes the type II/IV analysis much simpler. We modify the DP for the type I case to the form in Fig. 4*A*, where the translation vectors $\boldsymbol{t}_M$ and $\boldsymbol{t}_T$ lie in the plane of distortion and define the twin angle α and the TD vector $\boldsymbol{b}_g$ and the step height *h*. The partitioned glide vectors become $\boldsymbol{b}_{gM}$ and $\boldsymbol{b}_{gT}$, respectively, each with a magnitude equal to $\boldsymbol{b}_g$. The components of $\boldsymbol{b}_{gM}$ and $\boldsymbol{b}_{gT}$ parallel to *P* cancel and do not contribute to *b*. The components $\boldsymbol{b}_M$ and $\boldsymbol{b}_T$ in the glide plane sum to the net glide vector $\boldsymbol{b}_M + \boldsymbol{b}_T = \boldsymbol{b}_g$. Viewed normal to *P*, the relevant vectors all lie in the plane of distortion as shown in the view parallel to the plane of distortion (Fig. 4*B*). The view in Fig. 4*C* emphasizes that the *t* vectors reside in the plane of distortion. The vectors $\boldsymbol{b}_M$ and $\boldsymbol{b}_T$ are depicted along with the projections, $\boldsymbol{b}_{gMpr}$ and $\boldsymbol{b}_{gTpr}$ of the Burgers vectors and $\boldsymbol{t}_{Mpr}$ and $\boldsymbol{t}_{Tpr}$ of the translation vectors in the TD glide plane k_1. Note that these projections are on a different plane than those with subscripts Mp and Tp and so have distinctive subscripts. The edge components of $\boldsymbol{b}_{gM}$ and $\boldsymbol{b}_{gT}$ parallel to *P* cancel in the twin plane and are of no further consequence here. However, they are important in the mechanism of faceting of the twin when it occurs. Since the twinning element $\boldsymbol{\chi}_1$ is parallel to $\boldsymbol{t}_M$, it is rational, consistent with the classical model, but there is an added proviso for type I, as follows:

Principle 1. The twin where rational *t* vectors lie in the plane of distortion in a dichromatic pattern is defined as a type I twin. Then and only then is $\boldsymbol{\chi}_2$ rational.

When the reference vector $\boldsymbol{t}_0$ in Fig. 2*F* is normal to the TD glide plane, the $\boldsymbol{t}_M$ and $\boldsymbol{t}_T$ vectors always reside in the plane of distortion. This is true for many twins in high-symmetry crystals, so such twins are type I. For all triclinic crystals, the $\boldsymbol{t}_0$ vector is inclined to the TD glide plane, and one must examine $\boldsymbol{t}_M$ to determine whether $\boldsymbol{t}_{Mpr}$ is in the plane of distortion. Inclined $\boldsymbol{t}_0$ vectors are also present for twins on (010) planes in monoclinic crystals but not on (100) or (001) planes where the $\boldsymbol{t}_0$ vector is normal to the TD glide plane. Inclined $\boldsymbol{t}_0$ vectors are present for twins with {100} planes in trigonal crystals (the notations for directions and (hkl) for planes mean all directions or planes with h, k, and l permutated). Inclined $\boldsymbol{t}_0$ vectors are possible but uncommon in higher symmetry crystals.

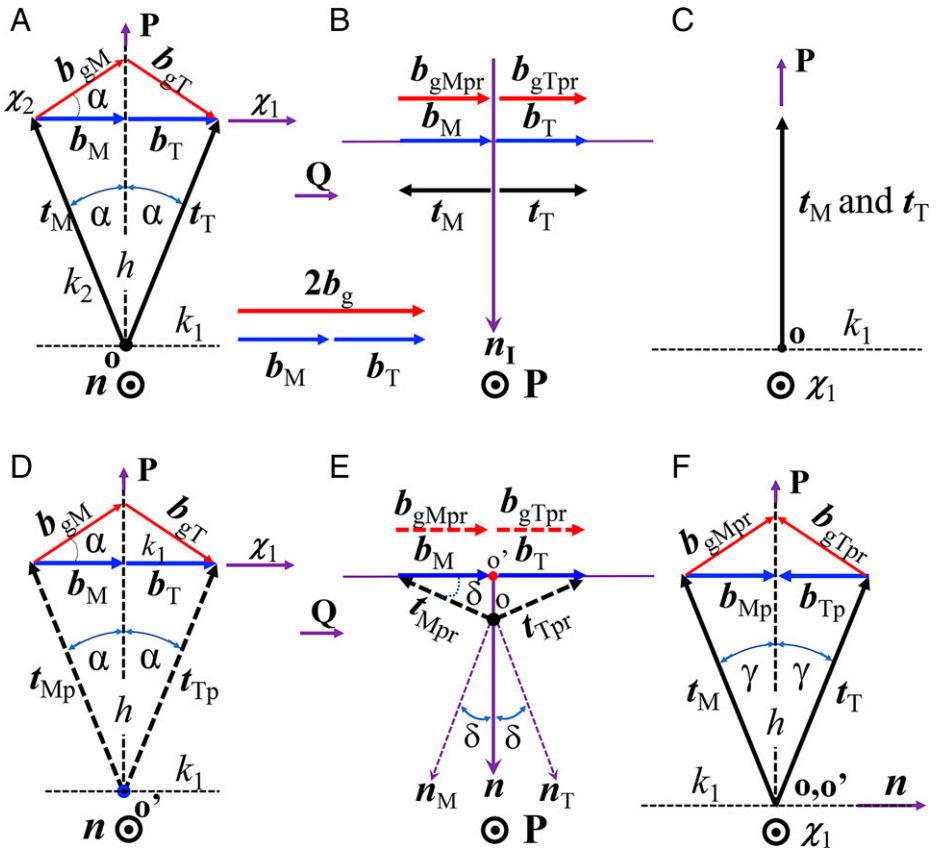

Fig. 4. (*A*) TM diagram for a type I twin. Translation vectors, partitioned glide vectors $\boldsymbol{b}_{gM}$ and $\boldsymbol{b}_{gT}$, and in-plane components $\boldsymbol{b}_M$ and $\boldsymbol{b}_T$ are shown. (*B*) View parallel to the plane of distortion showing the projections of the translation vectors and the Burgers vectors in the k_1 glide plane; the latter actually all superpose but are displaced for clarity. (*C*) View of *A* parallel to χ_1. The *t* vectors lie in the plane of distortion. (*D*) Equivalent of *A* for the type III case. Only the irrational components $\boldsymbol{t}_{Mp}$ and $\boldsymbol{t}_{Tp}$, indicated by dashed lines, lie in the glide plane. (*E*) Equivalent of *B* for the type III case. The translation vector components $\boldsymbol{t}_{Mpr}$ and $\boldsymbol{t}_{Tpr}$ in the plane of distortion are inclined by the angle δ to χ_1 (or *Q*). In plagioclase, $\boldsymbol{t}_{Mpr}$ is parallel to [101]. (*F*) View of *D* parallel to χ_1. The *t* vectors lie out of the plane of distortion.

Part of a DP for a generic type III case is shown in Fig. 4*D*. For type III, only the projections of the *t* vectors, indicated by dashed lines, lie in the plane of distortion. In Fig. 4 *E* and *F*, the origin of the *t* vectors then lies out of the plane of distortion. The components of $\boldsymbol{b}_{gM}$ and $\boldsymbol{b}_{gT}$ parallel to *n*, defining the angle γ, cancel and do not contribute to *b*. These projections define the twinning angle α.

$$\cos\alpha = (\boldsymbol{t}_{Mp} \cdot \boldsymbol{P}) / |\, \boldsymbol{t}_{Mp} \,| \,. \qquad [3]$$

The projection along *P* reveals the projections $\boldsymbol{b}_{gMpr}$ and $\boldsymbol{b}_{gTpr}$ of the glide vectors $\boldsymbol{b}_{gM}$ and $\boldsymbol{b}_{gT}$ in the TD glide plane k_1. The irrational projections of the translation vectors in the glide plane are $\boldsymbol{t}_{Mpr}$ and $\boldsymbol{t}_{Tpr}$, which are indicated by dashed lines. These projections define the twinning angle α. Because χ_1 is parallel to $\boldsymbol{t}_{Mp}$, which is irrational, the twinning element χ_1 is irrational for the type III case, in contrast to the classical theory as follows: the typical elements for type III are k_1 rational, and the other three elements irrational. The edge components of $\boldsymbol{b}_{gM}$ and $\boldsymbol{b}_{gT}$ parallel to *P* cancel as for type I. The vectors $\boldsymbol{b}_M$ and $\boldsymbol{b}_T$ have screw components as shown in Fig. 4*F*. However, these are equal and opposite and cancel so their sum, 2*b*, has no screw component.

The angle δ between $\boldsymbol{t}_{Mpr}$ and χ_1, shown in Fig. 4*E*, is a measure of the deviation of a type III twin from type I. Also, δ is given by the angle between $\boldsymbol{n}$ and one of the normals $\boldsymbol{n}_M$ or $\boldsymbol{n}_T$ to $\boldsymbol{t}_{Mpr}$ or $\boldsymbol{t}_{Tpr}$, as in Fig. 4*E*. This angle has no physical significance for a given crystal other than indicating the twin type. However, in plagioclase for example, values of δ vary with composition and are of interest in defining the relative deviations from type II. One can calculate δ from the relation:

$$\delta = \cos^{-1}(\boldsymbol{t}_{Mpr} \cdot \boldsymbol{b}_g) / |\, \boldsymbol{t}_{Mpr} \,||\, \boldsymbol{b}_g \,| \,, \qquad [4]$$

and the angle $\delta = 0$ for type I twins. In accord with this analysis, we define a type III twin as follows:

Principle 2. The case where no rational *t* vectors lie in the plane of distortion is defined as a type III twin. An equivalent statement is that χ_2 is irrational for a type III twin.

Type III Twins in Plagioclase. To further clarify the distinction between type I and type III twins, we consider plagioclase. The symmetric DP entails TDs with $h = 2h_0$ with $h_0 = [010]$ referred to the primitive unit cell. The double height primitive cell corresponds to the large unit cell often chosen for plagioclase (4, 7). The TD with $h = h_0$ would have an irrational origin, counter to the above conditions for the TM. If it existed, its Burgers vector would be half that of the symmetric case. Fig. 5 shows crystallographic models for Albite twins in three different plagioclase lattices. Fig. 5*A* is a three-dimensional (3D) portion of the DP for a type I twin. The three lattice sites shown as balls define the *t* vectors which lie in the plane of distortion, so the associated twin must be type I. The projection in Fig. 5*B* affirms that the *t* vectors are in a type I configuration. This figure defines the reference state with the angle $\delta = 0$ and the angle β_I representing the deviation of n_I from a low-index, rational direction. For one composition in labradorite, the lattice is monoclinic and the twin is type I for any *b* in the glide

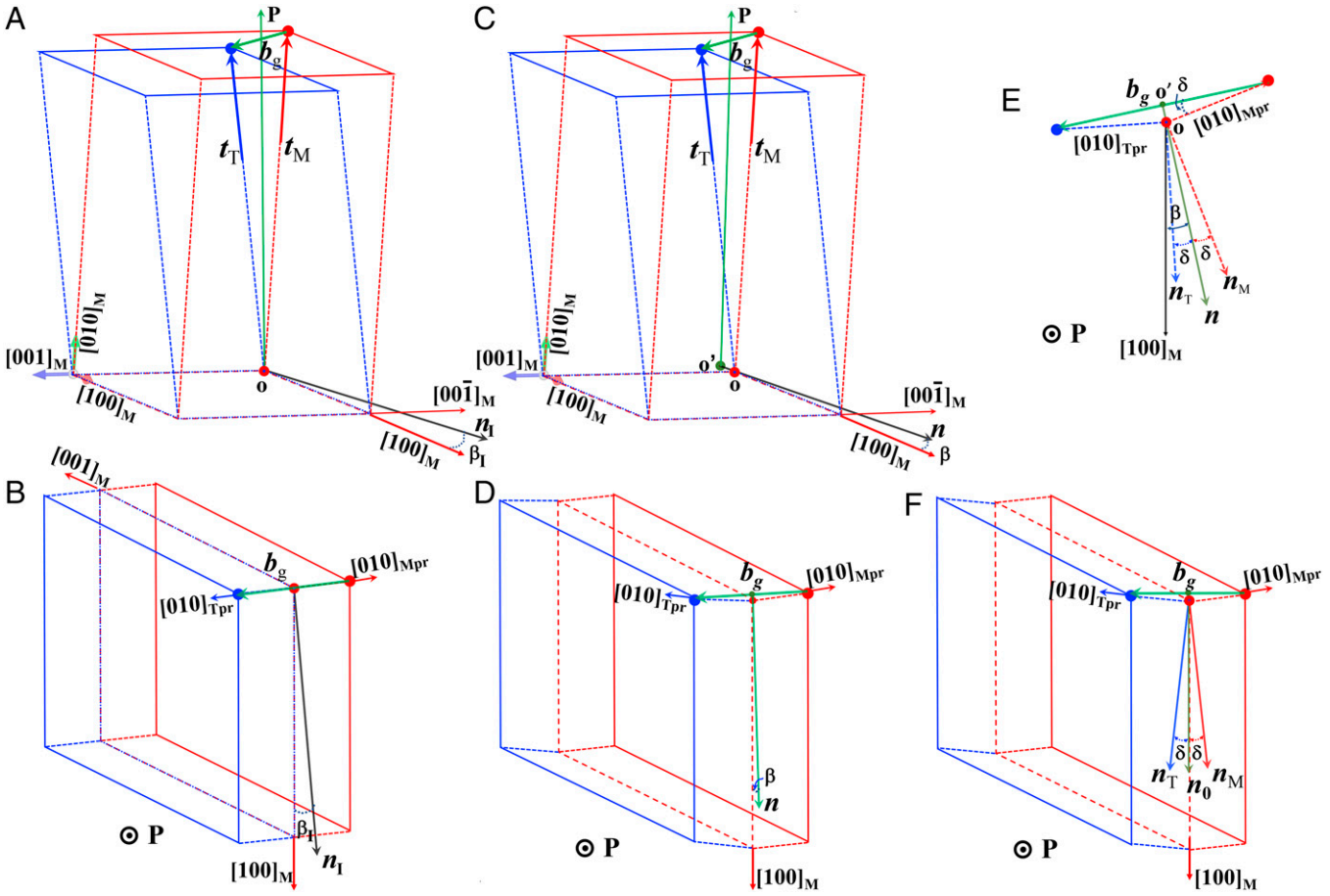

Fig. 5. (*A*) 3D DP for a generic triclinic crystal e-cell (or elementary transformation volume) (6), showing $\boldsymbol{b}_g$, $\boldsymbol{n}$, $\boldsymbol{t}_M = [010]_M$, and $\boldsymbol{t}_T = [010]_T$ for a type III twin. The three large balls sites represent sites like those in Fig. 4*A*. (*B*) Projection of the type I DP normal to P, showing $\boldsymbol{b}_g = \boldsymbol{b}_{gM} + \boldsymbol{b}_{gT} = \boldsymbol{b}_M + \boldsymbol{b}_T$ and $\boldsymbol{n}$. The small red balls represent sites in (010) plane that are displaced in the **-*P*** direction. (*C*) Projection of the type III DP normal to *n* with the Burgers vector $\boldsymbol{b}_g$ subtending an angle δ with the trace $\boldsymbol{t}_{Mpr} = [010]_{Mpr}$ of the $[010]_M$ direction on the glide plane. (*D*) View normal to *P* on the {010} glide plane showing the special case where $\boldsymbol{b}_g^0$ is normal to $\boldsymbol{n}_0 = [\bar{1}00]$. (*E*) The enlargement of *D*, showing *n* with the Burgers vector $\boldsymbol{b}_g$ subtending an angle δ with the trace $\boldsymbol{t}_{Mpr} = [010]_{Mpr}$ of the $[010]_M$ direction on the glide plane. (*F*) View normal to *P* on the {010} glide plane showing the special case where $\boldsymbol{n}$ is parallel to $[100]_M$ and $\beta = 0$.

plane. Fig. 5*C* is a 3D portion of the DP for a general type III twin. Consistent with Figs. 2*F* and 4*F*, the origin o′ for *P* is displaced from the nearby lattice site origin o. In Fig. 5*D*, the projection of the 3D DP, like that in Fig. 4*C*, is normal to the (010) glide plane, and the $\boldsymbol{t}_M$ and $\boldsymbol{t}_T$ vectors do not in the plane of distortion. The displacement of origin of P is emphasized in the enlargement in Fig. 5*E*, analogous to Fig. 4*E*. The vector $\boldsymbol{b}_g$ subtends an angle δ with $[010]_{Mpr}$ and is irrational, so the twin is type III. Fig. 5*F* is the special case of type III where the vector n_0 is parallel to the low-index direction $[100]_M$ so that $\beta = 0$ In general, therefore, β and δ are determined from

$$\beta = \cos^{-1}(\boldsymbol{n} \cdot \boldsymbol{n}_0). \qquad [5]$$

Since both β and δ rotate by the same amount relative to the reference state, the angle δ for the general case is given by

$$\delta = \beta - \beta_1, \qquad [6]$$

an alternative to Eq. **4**.

Fig. 5 also applies for the TD glide that is the first stage in forming types II and IV twins. A key point is that the partitioning in Fig. 5*C* entails only displacements in the plane of distortion. Consequently, if the first stage glide is the same as for a type I twin, the *t* vectors lie in the plane of distortion and the twin is type II. Analogously, if the first stage glide is for a type III twin, there will be no rational *t* vectors after partitioning either. Thus, the twin is type IV. In the monoclinic limit that the lattice parameter γ_0 is 90°, all triclinic twins with precursors oriented as in Fig. 3 become type II. In monoclinic crystals, twins on (010) are type IV, but for other twin planes such as (100) or (110), type I is probable because the lattice parameters α_0 and β_0 are 90°. While rarer in higher symmetry structures, type IV is possible.

SI Appendix, Table 1 summarizes the lattice parameters (28) and *SI Appendix*, Tables 2 and 3 summarize the TD parameters and the angles α, β, and δ for plagioclase twins of varying compositions. Because there is no experimental evidence for the general case where $\beta \neq 0$, we assume that the implied case where $\beta = 0$, Fig. 5*D*, applies. The values for the $\beta = 0$ case are likely upper bounds for δ. The atomic arrangements near the twin plane suggest that the actual value of β may be intermediate between these two extremes. Aside from compositions near labradorite, the differences between the type I/II approximations and the type III/IV values are quite marked, with δ values ranging up to 33°.

Symmetry for Type I/III Twins. Type I twin planes were recognized as crystallographic mirror planes in the earliest descriptions (1, 23). Pond (29), in the topological theory, formalized this concept for type I and II twins by highlighting symmetry operations (denoted with apostrophes in the symbols) that are not those of the matrix crystal lattice but are added symmetry elements in the DP that help in envisioning the interface as a twin. The symmetry of the

pattern is the union of the symmetries of the two crystals and many of the single crystal symmetry operations, such as translation, are broken in the DP used as a reference for any twin (29). At the same time, with the broken symmetry as a basis, the DP can acquire some elements such as a twofold axis 2′. The TM model applies only when the terrace plane, here the twin plane, is commensurate or, equivalently, if the dividing surface in the DP is commensurate. Therefore, for type I twins in both the classical model and the topological theory, the dividing surface in the DP is always a mirror plane m' as is the twin (composition) plane. Correspondingly, there is always a rotation axis 2′ parallel to the direction P. This is true if triclinic crystals have a center of symmetry and for all other crystal systems. In special high-symmetry crystals, $Q||\boldsymbol{\chi}_1$ can also be a rotation axis 2′. For example, Q is a 2′ axis because $\boldsymbol{\chi}_1$ is parallel to $[10\bar{1}1]$ in a hexagonal close packed structure (30, 31). In most twins, $\boldsymbol{\chi}_1$ is irrational. Other symmetry elements can be present is special cases. Hence, in the TM, the type I interface is always a mirror plane in the DP. As mentioned previously, when $\boldsymbol{p} \neq 0$, the m' and 2′ symmetries are broken in the SDP and in the twin $\boldsymbol{p}$ is rarely known, so this has little impact in practice. More details are presented in *SI Appendix, Matrix description of the twin in the TM*.

Because twins in most metals and simple compounds are type I or II, the conventional expectation was that all twins, including growth twins, had mirror symmetry. Yet, there is no m' symmetry for type III twins. As an example, for most triclinic crystals such as the plagioclase considered here, principle 1 is not satisfied and the crystallographic symmetry is reduced from the type I/II case as shown in Fig. 4. There is no m' symmetry but P remains a 2′ axis. Misleadingly, the twinning displacements u have tilt-like symmetry as in Fig. 2*F*, but there is no crystallographic m' symmetry. The false symmetry implied by Fig. 3*F* would not be present in 3D. Only if $\boldsymbol{\chi}_1$ was parallel to the $\boldsymbol{t}_{\mathrm{Mp}}$ direction would a triclinic twin be type I with (001) being a m' plane. As far as we know, no triclinic crystals have this topology. Yet, the mechanism for types III and IV, including TDs with partial dislocation Burgers vectors, is analogous to the general behavior for type I or II twins. Because the mechanism is similar, we retain the twin terminology but define types III and IV to emphasize the differences from types I and II. The resultant symmetry is consistent with the general treatment of possible twins in refs. 21 and 22. These symmetry concepts all apply only to perfect twin planes or terraces and only to type I to IV twins.

When the $\boldsymbol{t}_0$ vector is normal to the glide plane, the $\boldsymbol{t}_{\mathrm{M}}$ and $\boldsymbol{t}_{\mathrm{T}}$ vectors both always lie in the plane of distortion. This condition is met in many high-symmetry materials so the twins for such crystals are always type I/II as defined here. The macroscopic orientation relationship, denoted generally as the OR, is 2α for any among the types I to IV.

The Physical Model for Type II/IV Twinning

A mechanism for type II twinning entailing TD glide on a plane k_1, equivalent to K_2, was suggested in ref. 9 and developed in detail in terms of the TM in refs. 10, 12, and 13. A hypothetical reversible path demonstrating the type II/IV mechanism for any crystal undergoing deformation twinning is presented in Fig. 6. As indicated in Fig. 6*A*, a single crystal is cut into what will become the matrix and twin. Disconnection glide in the twin produces plastic engineering strains and offsets of the surfaces (Fig. 6*B*). If the shear was not accommodated by rotation, there would be a large incompatibility with accompanying stresses. As shown in refs. 12 and 15, the incompatibility is removed by partitioning the displacements, occurring by a rotation of the interface by α, relative to both twin and matrix, resulting in the total symmetrical rotation of the twin in Fig. 6*C* by 2α The true physical process (15, 18, 19) is shown in Fig. 6 *E*–*G*, which relate the model to the twinning elements. Fig. 6*E* shows the precursor glide on k_1, with a resultant stressed array of edge dislocations on a nonequilibrium interface. The nonpartitioned angle between k_1 and k_1' is the simple shear angle $2\alpha'$. Also depicted is the partitioning rotation R, achieved by interface rotation, that creates the equilibrium twin boundary k_2, presented in Fig. 6*F*. Because the plastic strain is partitioned, the state of strain is different and α differs from α' (15, 19). If the tilt wall terminates, incompatibility stresses are present at the tip. These can be removed by emissary dislocations creating a stress-free boundary $k_{2\,rec}$ normal to $k_{1\,rec}$ shown in Fig. 6*G*. This entails the antirotation $\boldsymbol{R}_{\mathrm{rec}} = -\alpha$. The result for a cuboidal twin with one set of TDs is three orthogonal twin interfaces, $k_{2\,\mathrm{rec}}$, $k_{1\,\mathrm{rec}}$, and a twist boundary, with a uniform orientation relationship equal to 2α (17) for all three boundaries.

In a hypothetical process, e could directly partition into two symmetrical portions $e/2 = \tan\alpha$, as in Fig. 6*B*. In an actual process, this might not be possible. As an example, for unit TDs, the physical engineering shear e cannot partition in this way because this would require a TD partial on every other plane, resulting in profuse stacking fault formation. Yet, the final configuration for the hypothetical partitioned process, shown in Fig. 6*C*, corresponds to the real twin in Fig. 6*D*. The effect of partitioning is that the final configuration is such that the true engineering strains are partitioned as in the hypothetical process. Hence, the final twin has partitioned engineering strains, crystal structure, and rotations.

For TDs with multiple step heights, e could partition physically in plagioclase or any other crystal. For example, in face centered cubic structure the unit TDs have b of the type $1/6\langle 112\rangle$, while those bounding extrinsic faults have $h = 2h_0$. The latter TDs could have a net $b = 1/6[112]$ but locally split into two different Burgers vectors such as $1/6[2\bar{1}1]$ and $1/6[\bar{1}21]$ (e.g., figure 10.8 in ref. 27).

The details of the type II/IV twinning model in any crystal are depicted in Fig. 7. The TDs nucleate and glide on k_1, accumulate in a planar array, and then rotate to form a tilt wall corresponding to a type II or IV k_2 interface.

The Topological Model for Type II/IV Twinning

Fig. 8*A* is similar to the diagrams in Fig. 4. Fig. 8*B* is a portion of the DP for a type II twin in any crystal. A useful reminder is that the DP in Fig. 8*B*, the TM extension of Fig. 6*F*, comprises an extension of the twin lattice sites into the matrix and vice versa. For type II, $\boldsymbol{t}_{\mathrm{M}}$ and $\boldsymbol{t}_{\mathrm{T}}$ initially coincide in the plane of distortion. With partitioning, they rotate oppositely by $\pm\alpha$ into the matrix and twin and their vector sum yields the tilt Burgers vector (Fig. 8*C*). Thus, Fig. 8*B*, along with Fig. 6*F*, reveals that neither t vector resides in the interface; they are both rotated from the interface by the angle α As a consequence, $\boldsymbol{\chi}_2$ is irrational, and the type II TM result almost never agrees with the classical result. While it is true that this result would agree with the classical result in the limit $\alpha \to 0$, there would be no twin in that limit. The only exception is when α is so large that another low index plane rotates into the k_1 plane; an example is the {111} type II twin in face centered cubic crystals, where $\alpha = 35°\ 16'$. Therefore, we redefine a type II twin as follows:

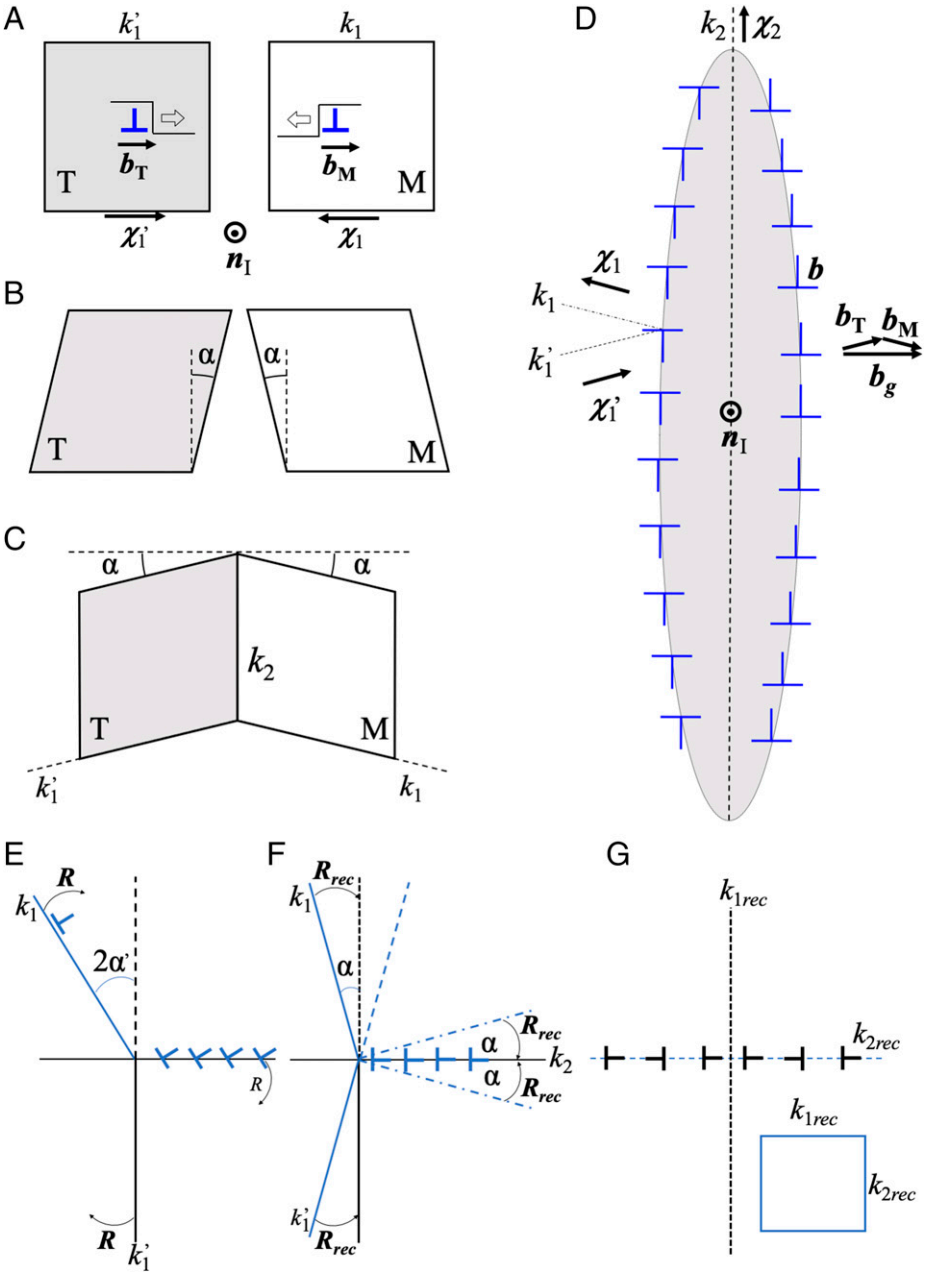

Fig. 6. Hypothetical reversible path to form a type II or IV twin. (*A*) TDs with Burgers vectors $\boldsymbol{b}_T$ glide on the k_1 plane in both the twin and matrix. (*B*) Glide produces engineering shear of the twin and matrix. (*C*) The crystals are rotated and form a type II twin. (*D*) Type II or IV twin, rotated from preceding figures by 90°. (*E*) Simple shear portion of the type II mechanism. Rotation to achieve partitioning are shown. (*F*). Final equilibrium structure. (*G*) Rotation 2α removed by emissary dislocations leaving a boundary with no net Burgers vector content.

Principle 3. A type II twin is defined by the rational TD glide plane $k_1 = K_2$ and rational translation vectors $\boldsymbol{t}_M$ and $\boldsymbol{t}_T$ vectors in the plane of distortion.

For the case in Fig. 8*B*, the vectors $\boldsymbol{t}_{\mathrm{M}}$ *and* $\boldsymbol{t}_T$ lie in the plane of distortion and the twin is type II. For the type IV case in Fig. 8*D*, the t vectors are rational but their projections $\boldsymbol{t}_{\mathrm{Mp}}$ and $\boldsymbol{t}_{\mathbf{Tp}}$ onto the plane of distortion are irrational and χ_2 is irrational. Thus, we define a type IV twin by the following:

Principle 4. A type IV twin is defined by the rational TD glide plane $k_1 = K_2$ and t vector projections $\boldsymbol{t}_{Mp}$ and $\boldsymbol{t}_{Tp}$ that are irrational in the plane of distortion.

The final TM result is a set of double tilt dislocations spaced at a distance $2L$ in the k_2 plane. The actual boundary an array of single tilt dislocations as shown in Fig. 8*E*.

With the above principles, we can also define conjugate pairs as follows:

Principal 5. Conjugate pairs, whether I/II or III/IV have the same α.

Correspondingly, they have the same OR, the crystallographic description of the relative rotation between twin and matrix. Only in high-symmetry I/II cases does this imply that the Miller indices are interchangeable in the sense that direction/plane becomes plane/direction in the conjugate, as often observed for compound twins.

Another aspect of the classical analysis of type II, as indicated for minerals (26–29, 32), is that the normal to the plane of distortion is thought to be a low index direction, so that the k_2 plane has indices $\{h0k\}$. The reason for that is that χ_2 is defined as a conjugate having low-index Miller indices in the classical model. With the new definition of type II, a low-index χ_2 is impossible except for high-symmetry cases, which have not been found for triclinic systems. Here, the k_2 plane has

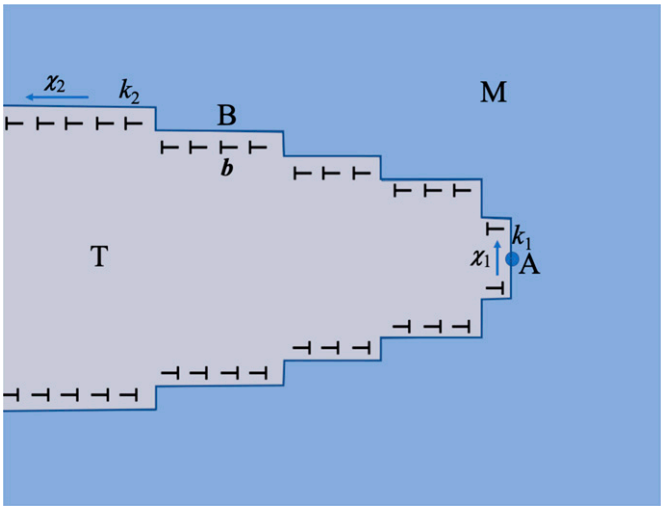

Fig. 7. TDs with vector b_g nucleate at *A*, glide, and accumulate. The Burgers vector rotates into the tilt configuration *b* at *B*, eventually creating the type II or IV twin boundary k_2.

indices $\{h0k\}$ only for the special case in Fig. 5*D*, and only type IV twins can have this special orientation of k_2. More commonly, as for the plagioclase crystals in *SI Appendix*, Table 3, the type IV twins have the form $\{hkl\}$. Nonetheless, type II and IV twins share the same k_1 plane and form from the same TDs, respectively, as is the case for types I and III.

For either type II or IV, there are only edge components to $\boldsymbol{b}_{\mathrm{M}}$ and $\boldsymbol{b}_{\mathrm{T}}$ The in-plane edge components cancel but the out-of-plane edge components add to give $2b$.

$$\boldsymbol{b} = (\boldsymbol{b}_{\mathrm{M}} + \boldsymbol{b}_{\mathrm{T}})/2,\ b = b_{\mathrm{M}} \cos \alpha. \qquad [7]$$

For type IV, the angle α is rotated and larger than for the type II case, and χ_2 is rotated relative to the type II result. The twinning elements for types III and IV are k_1 rational, and the other three elements are irrational.

Observations of Type III/IV Twinning

Plagioclase has a triclinic crystal structure with Pericline twins classically treated as type II. Fig. 1*B* shows a tilt disconnection for a Pericline twin in labradorite. The analysis of this twin indicates that it is instead type IV, with $\beta = 0$ and $\delta \neq 0$, as shown in *SI Appendix*, Table 3. However, for compositions near labradorite, the lattice parameter γ_0 is so close to 90° that the structure is nearly monoclinic, and the twins are effectively type II for any value of β. *SI Appendix*, Table 3 shows that the Pericline twins with $\beta = 0$ in other plagioclase minerals are definitely type IV, differing significantly from type II. In bytownite, we have determined α directly by Kikuchi line analysis and proved unequivocally that the Pericline twins are type IV with $\beta = 0$. The values of α and β for Pericline twins are quite important for examples where the type II or IV plane is faceted.

The present analysis indicates that they are instead type IV. The Pericline twins in plagioclase all have values of δ that are nonzero, so the twins are type IV. However, for compositions near labradorite, the lattice parameter γ_0 is so close to 90° that the structure is nearly monoclinic, and the twins are effectively type II. The discrepancies from classical theory could also apply for some twins in materials with higher symmetry. Albite twins in plagioclase were identified as type I twins (5, 32). Our earlier work (9, 23) followed that nomenclature, but in retrospect, there was a nonzero value of δ. Hence, the present analysis indicates instead that the Albite twins are type III. The Albite twins in labradorite, however, are approximately type I because the crystal structure is effectively monoclinic. When available, the elements k_1 and χ_1 suffice to determine all twinning elements. There are extensive data for k_1, but little data exist for χ_1. Additional measurements would be valuable.

Another example is one type of twinning in NiTi, analyzed as type II (18, 19, 23). In refs, 18 and 19, the TM analysis properly used the symmetrical structure shown in Fig. 2*E* rather than the classical structure shown in Fig. 2*B*, but the small nonlinear corrections in ref. 23 were not included. Thus, $\boldsymbol{b}_g$, n, h, and α are the values in ref. 23, and essentially those in ref. 19, based on known experimental results for the twinning elements (33). Fig. 9*A* is a 3D DP. Fig. 9*B* is a portion of the DP projected normal to the (110) glide plane, the type I precursor. Fig. 9*C*, blown up near the origin, clearly shows that the nearest t vectors, of the [110] type, do not lie in the plane of distortion; the twin is type IV, not type II. Thus, the key parameters are $\alpha = 3.916°$, $\beta = -7.34°$, $\delta = 17.54°$, and $b = 0.082$ nm. The TD Burgers vector has magnitude of $b_g = b \sec \alpha = 0.086$ nm It is impossible for the twins in NiTi to be type II unless o = o' so that $\delta = 0$. With these false values, $\delta = 0$ and $b = 0.086$ nm, the other key parameters would be $\alpha = 3.991°$ and $\beta = 10.21°$. Fig. 9*D* is the view along P after the partitioned rotations to create type IV have been imposed. This view defines the plane $k_2 = (1.00, 0.814, -0.7594)$ and $\chi_2 = [1.00, 0.3213, -0.3213]$. While we have modified the earlier analysis (20) in that the twin is type IV, the fact that the correct type IV parameters b, n, h, and α were presented reinforces the finding that the TM and Fig. 2*E* always yield the correct results, knowing b_g and h. The present TM analysis gives the proper twinning elements, orientation relationships, and TD in agreement with ref. 26 and nominally with ref. 19. The classical type II analysis would give inaccurate results for these quantities and would complicate the analysis of faceting when it is present.

A preliminary consideration indicates that the twins in triclinic devitrite (34), a $Na_2Ca_3Si_6O_{16}$ silicate (35), are type IV twins, while those in trigonal mercury (36) are type II. Possibly, other observations of twinning modes cited as type I or II may be type III or IV when analyzed in the present version of the TM.

Differing from those discussed here, there are other situations where several elements are irrational, reviewed in ref. 15. One example is the formation of irrational k_1 and k_2 planes by double twinning. Another is that the twinning direction becomes irrational when two TDs with different b_g vectors operate on the same glide plane. An example is $(10\bar{1}1)$ twinning of type I in hexagonal close packed crystals (37). This case could still be treated as in section *The Physical Model for Type II/IV Twinning*, but with b_g replaced by the average $\langle \boldsymbol{b}_g \rangle$ parallel to χ_1.

Discussion

There are two major thrusts in this work. First, the simple shear of the classical model yields the disconnection parameters b and h. These suffice to describe type I twins in either the classical or TM models. However, for type II, the distortion is a simple shear plus a partitioned rotational distortion (15, 18, 19), and the classical model only applies in a linear plastic description (19, 23). To include the symmetrical partitioned distortion, the use of the symmetric displacement description in Fig. 2*E*, as

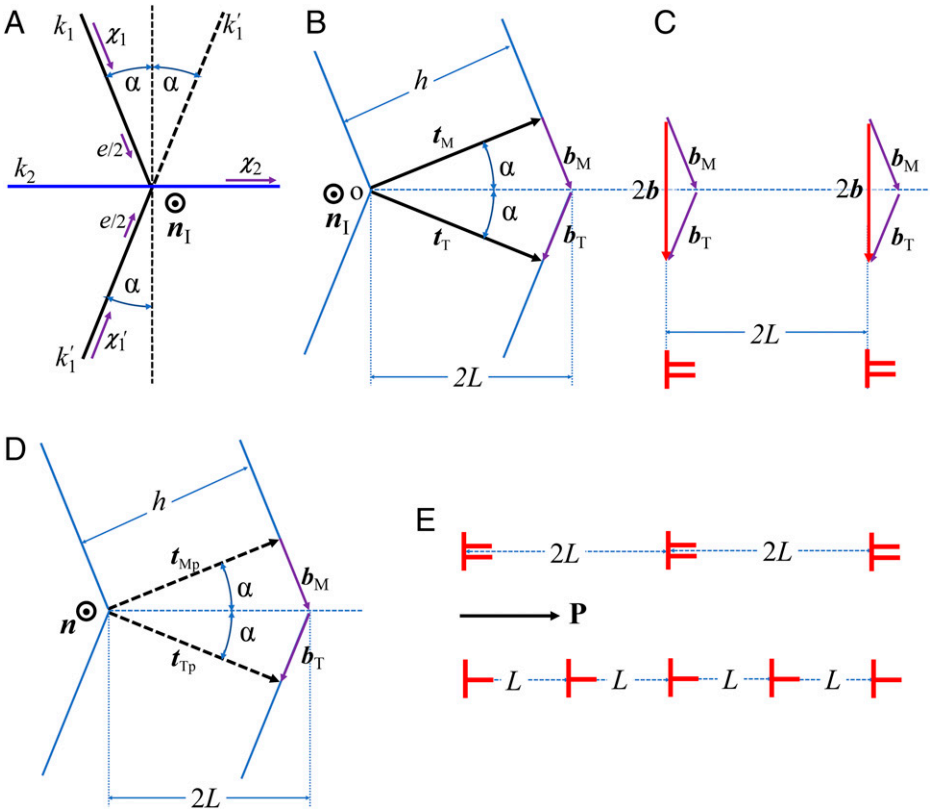

Fig. 8. (*A*) View normal to the plane of distortion for a type II or IV twin. Engineering strains with partitioned rotations produce a type II or IV twin with a rotation angle α. (*B*) Initially, for type II, $\boldsymbol{t}_M$ and $\boldsymbol{t}_T$ coincide in the plane of distortion. With partitioning, they are rotated symmetrically into the matrix and twin. The resultant k_2 plane is irrational the twin is type II with tilt Burgers vector 2*b*. (*C*) View showing the partitioned Burgers vectors that sum to the tilt vector 2*b* of tilt dislocations separated by the distance 2*L* on the twin plane. (*D*) If the *t* vectors are not in the plane of distortion, the twin is type IV with tilt Burgers vector 2*b*. The angle α is determined by the components of the *t* vectors projected onto the plane of distortion. (*E*) Relaxation to single defects by the rigid shift of the twin by *p* with magnitude *L*.

done in the TM, is imperative. Second, when the unit cell axis normal to the twinning plane is inclined obliquely, as in many low symmetry crystals χ_1 can be irrational, so accompanying twins are types III and IV.

Hence, we have introduced definitions of type I twins, consistent with the classical model, and type II twins, which differ from the classical model. In addition, we have described type III and IV twins that differ from types I and II. The tables in *SI Appendix, Matrix description of the twin in the TM* verify principle 3, as follows: the classical definition of a rational χ_2 for a type II twin is impossible. Type II requires that $\delta = 0$, but then $\beta \neq 0$. Also, if $\beta = 0$ and then $\delta \neq 0$. Incorrect Burgers vectors for TDs and the twinning direction χ_1 would be predicted. Thus, compilations of twinning elements with both angles zero can at best only be approximate. With this definition, type II is possible and applies to a fair approximation for labradorite since γ_0 is close to 90°.

With reported χ_1 values, *SI Appendix*, Table 3, δ values range up to 33° so the difference between types I/II and III/IV can be substantial. Specifically, Albite twins in plagioclase are shown to be examples of type III twins. Pericline twins in plagioclase and $(0\bar{1}1)$ twins in NiTi are shown to be type IV twins. If type III twins are assumed to be types I, the wrong Burgers vectors for TDs and twinning direction χ_1 would be predicted. If type IV twins are assumed to be type II, the incorrect parameters would be TD Burgers vector, k_2, χ_2, and *e*. With either assumption, there would be imprecision in the twin description and in the analysis of the contribution of twinning to plastic deformation.

A major difference for type III/IV twins is the absence of m' and $2'$ symmetry. This is contrary to expectation for twins in simple high-symmetry crystals. Still, there is a logical basis for the lack of symmetry. The twinning direction χ_1 is determined by the minimum activation energy path. In metals with high symmetry, central forces dominate the energy of the twin plane and activation path. The saddle point often lies in a symmetrical direction as does the TD Burgers vector, e.g., [112] for face centered cubic structure. The result is mirror symmetry for the twin. In contrast, minerals have strong directional bonding and many atoms per lattice site with only c' point symmetry. As an example, there are 26 atoms per lattice site for plagioclase. Hence, there is no reason for either the minimum on a gamma surface or the activation path to lie in a low index direction. Therefore, there is no fundamental reason why *b* or χ_1 should always lie in a low index direction, so that type III/IV twins are not unexpected. Also, these III/IV twins cannot have m' and $2'$ symmetry. We emphasize that the absence of mirror symmetry is consistent with the general analysis of possible twinning elements (19, 22). The analysis of the Albite–Carlsbad twins in plagioclase (7) is a specific example of rotation indicating the absence of $2'$ symmetry.

Other than modifying the definition of type I and introducing type III, there is no mechanistic significance of the present analysis for type I. For type I in conjugate systems, the prediction that the conjugate is type II is valid only with the definition of type II introduced here. Type III is of critical importance, however, in describing the precursor for types II and IV twinning. These concepts are also important in understanding faceting of twin planes and large steps or disconnections on twins. After the details are

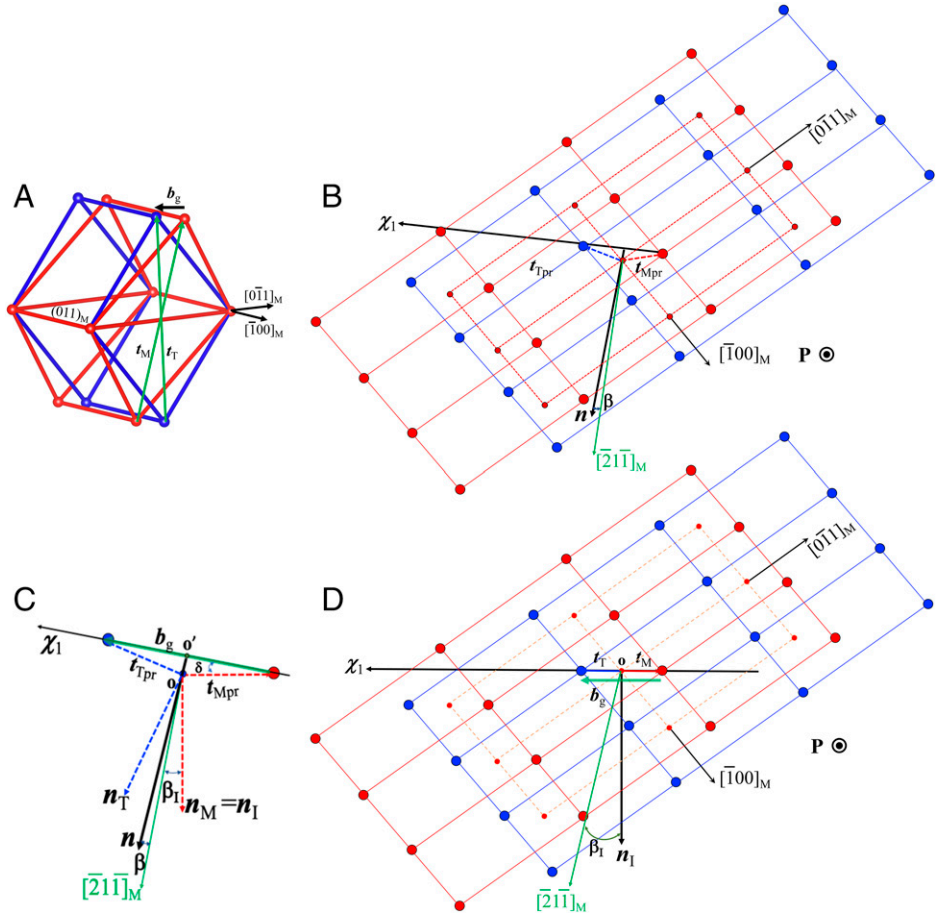

Fig. 9. (*A*) 3D DP for NiTi. (*B*) Projection of the DP normal to the glide plane. The small red and blue circles represent lattice sites in the layer below the origin, and the big red and blue circles are in the layer above the origin. (*C*) Detail of *B* showing the origin displaced from a lattice site as in Fig. 4*D*. The dashed lines indicate that only the components $\boldsymbol{t}_{Mpr}$ and $\boldsymbol{t}_{Tpr}$ lie in the plane of distortion. The angle β is also shown. (*D*) Projection of the type I DP normal to *P*.

established, one need not study the DPs such as those in Fig. 5 in detail. A simple procedure is to construct Figs. 3*E* or Figs. 4 *C* and *D* and calculate α, β and δ from Eqs. **1** and **2** as in the plagioclase example. Many twins are type I or II in high-symmetry crystals. In low-symmetry structures such as triclinic, type III or IV twins are more likely.

The earlier TM analyses (17, 18, 23) for the examples presented here are correct only in the type II approximation that $\boldsymbol{t}_M$ lies in the plane of distortion. They also were described by the classical definition of type II instead of the definition here in principle 2. They do differ from the classical theory because both the topological theory (29) and the TM (38) included the symmetric configuration in Fig. 3*E* rather than the asymmetrical Fig. 3*B*. The present version of the TM model removes the approximation and results in different twins of types III and IV. The differences essentially arise from the dual mechanism of engineering shear plus rotational partitioning for type II/IV twins. Specific differences from the earlier work include modified α values; the I, III or II, IV nomenclature; the significance of the n direction; and the addition of the angles β and δ.

The introduction of these concepts provides ways to interpret the microstructural evidence for plastic deformation preserved in plagioclase at different geologic conditions. In general, the activation of twinning provides a way to accommodate the von Mises strain compatibility criterion at lower homologous temperature conditions where limited slip systems are active. The variation of twinning parameters with composition (and therefore symmetry) in plagioclase suggests that the activation energy for twinning could also change with composition, leading to variations in yield strength at conditions near the brittle-plastic transition in the crust. As plagioclase is a dominant phase in the crust of the Earth, Moon, Venus, and Mars, further work in this area could improve our understanding of deformation mechanisms in the lithospheres of all these planetary bodies. Twinning can accommodate low strain deformation in the lithosphere associated with flexural loads or off-fault plasticity associated with the propagation of earthquake rupture at the base of the seismogenic zone. Kink bands are common in highly anisotropic minerals such as micas and clays, as well as olivine, the dominant mineral in Earth's lithospheric mantle, deformed at low homologous temperature. The kink bands can be treated like the type I to IV twins using the above TM model, with the only difference being that perfect dislocations replace partial dislocations in the disconnections.

Transformation disconnections for shear type phase transformations have b components both in and normal to the habit. The latter entails rotational partitioning analogous to that treated here, accounting for differences in the TM from the classical phenomenological theory. Thus, the applications of the TM in such cases provide indirect support for the model presented here, and vice versa.

The results here have implications for constitutive modeling of deformation of minerals and other low-symmetry crystals, e.g refs. 39–42. The differences in α between *SI Appendix*, Tables 2 and 3 indicate that the strain tensor for a twin could be inaccurate if types I/II are assumed when types III/IV are appropriate.

Summary

In triclinic and some monoclinic crystals, because of the reduced symmetry, type IV twins form that are analogous mechanistically to type II twins. Similarly, type III twins form that are analogous to type I twins. The resultant twinning elements are determined by the topological model. The twinning mechanism is described in the topological model for type III as the glide of TDs on the k_1 plane and for type IV as the same glide plus the formation and relaxation of a tilt wall. Pericline twins in plagioclase are shown to be an example of type IV twins, and Albite twins are found to be type III. These type IV and III twins are characterized by irrational directional elements χ_1 and χ_2 and an irrational twin plane, $\{hkl\}$.

The TM type II twin never agrees with the classical description and we redefine a type II twin. The type I TM twin only agrees approximately with the classical result in the small twin angle limit. The crystallographic symmetry for type III/IV twins is shown to differ markedly from the type I/II cases.

Accounting for the variations in twinning mechanisms with composition (and therefore symmetry) of plagioclase can improve our understanding of plastic deformation of these important minerals at low homologous temperatures in the crust of planetary bodies.

Twins in known triclinic systems (4, 5, 26) are types III/IV, although twins in labradorite are approximately types I/II. For all known triclinic systems and some monoclinic systems, there is tilt-like symmetry of the displacements in forming the twin, but there is no crystallographic mirror symmetry across the twin plane.

Twinning is prevalent in many minerals, where slip is limited because Burgers vectors tend to be large. Hence, the same type IV mechanism may apply to other twin cases in such minerals and possibly in simpler structures such as metals, where there are some type II twins. The limitation would be that the χ_2 direction is irrational.

Data Availability. All study data are included in the article and/or *SI Appendix*.

ACKNOWLEDGMENTS. We are pleased to acknowledge support from the US NSF (CMMI-1661686 to J.W. and EAR-1624178 to G.H.). The reviewers' comments were most helpful.

1. Mügge, Beiträge zur kenntniss der structurflächen des kalkspathes und über die beziehungen derselben untereinander und zur zwillingsbildung am kalkspath und einigen anderen mineralien. Neues Jahrb. für Mineral. *Geol. und Palaeontol.* **1**, 32–54 (1883).
2. J. W. Christian, S. Mahajan, Deformation twinning. *Prog. Mater. Sci.* **39**, 1–157 (1995).
3. M. V. Klassen-Neklyudova, *Mechanical Twinning of Crystals*, J. E. S. Bradley, Ed. (Consultamts Bureau, New York, 1964).
4. H. R. Wenk, A. Bulakh, *Minerals: Their Constitution and Origin* (Cambridge University Press, Cambridge, 2016).
5. J. V. Smith, W. L. Brown, *Feldspar Minerals: Volume 1 Crystal Structures, Physical, Chemical, and Microtextural Properties* (Springer, Berlin, 2012).
6. I. J. Beyerlein, X. Zhang, A. Misra, Growth twins and deformation twins in metals. *Annu. Rev. Mater. Sci.* **44**, 329–363 (2014).
7. J. Hirth, J. Wang, G. Hirth, The topological model of defects and interfaces in complex structures. *Am. Mineral.* **104**, 966–972 (2019).
8. J. P. Hirth, G. Hirth, J. Wang, Disclinations and disconnections in minerals and metals. *Proc. Natl. Acad. Sci. U.S.A.* **117**, 196–204 (2020).
9. D. Xie, G. Hirth, J. P. Hirth, J. Wang, Defects in deformation twins in plagioclase minerals. *Phys. Chem. Miner.* **46**, 959–975 (2019).
10. R. Bürgmann, G. Dresen, Rheology of the lower crust ad upper mantle: Evidence from rock mechanics. *Annu. Rev. Earth Planet. Sci.* **36**, 531–567 (2008).
11. L. Mehl, G. Hirth, Plagioclase preferred orientation in layered mylonites: Evaluation of flow laws for the lower crust. *J. Geophys. Res.* **113**, B05202 (2008).
12. R. C. Pond, X. Ma, Y. W. Chai, J. P. Hirth, "Topological modelling of martensitic transformations" in *Dislocations in Solids*, F. R. N. Nabarro, J. P. Hirth, Eds. (Elsevier, Amsterdam, 2007), vol. **13**, pp. 225–262.
13. J. P. Hirth, R. C. Pond, R. G. Hoagland, X. Y. Liu, J. Wang, Interface defects, reference spaces and the Frank-Bilby equation. *Prog. Mater. Sci.* **58**, 749–823 (2019).
14. A. Ostapovets, A. Serra, Review of non-classical features of deformation twinning in hcp metals and their description by disconnection mechanisms. *Metals (Basel)* **10**, 1134–1154 (2020).
15. J. Wang, J. P. Hirth, C. N. Tomé, Disconnections and other defects associated with twin interfaces. *Prog. Mater. Sci.* **83**, 417–492 (2018).
16. R. C. Pond, J. P. Hirth, Defects at surfaces and interfaces. *Solid State Phys.* **47**, 287–365 (1994).
17. F. C. Frank, Crystal dislocations-elementary concepts and definitions. *Philos. Mag.* **42**, 809–819 (1951).
18. R. C. Pond, J. P. Hirth, Topological model of type II deformation twinning. *Acta Mater.* **151**, 229–242 (2018).
19. R. C. Pond, J. P. Hirth, K. M. Knowles, Topological model of type II deformation twinning in NiTi martensite. *Philos. Mag.* **99**, 1619–1634 (2019).
20. R. W. Cahn, Plastic deformation of alpha-uranium; Twinning and slip. *Acta Metall.* **1**, 49–70 (1953).
21. B. A. Bilby, A. G. Crocker, The theory of the crystallography of deformation twinning. *Proc. R. Soc. Lond. A Math. Phys. Sci.* **288**, 240–255 (1965).
22. M. Bevis, A. G. Crocker, Twinning shears in lattices. *Proc. R. Soc. Lond.* **304A**, 123–134 (1968).
23. J. P. Hirth, J. Wang, Extension of the classical theory for types I and II twinning. *J. Mater. Res.* **36**, 2615–2622 (2021).
24. H. A. Khater, A. Serra, R. C. Pond, Atomic shearing and shuffling ac- companying the motion of twinning disconnections in zirconium. *Philos. Mag.* **93**, 1279–1298 (2013).
25. O. Hardouin Duparc, A review of some elements for the history of mechanical twinning centred on its German origins until Otto Mügge's K_1 and K_2 invariant plane notation. *J. Mater. Sci.* **52**, 4182–4196 (2017).
26. B. Li, K. M. Knowles, Molecular dynamics simulation of Albite twinning and Pericline twinning in low albite. *Model. Simul. Mater. Sci. Eng.* **21**, 055012 (2013).
27. H. Borgland, H. Handlin, Experimental deformation of crystalline rocks. *Tectonophys.* **3**, 249–368 (1966).
28. I. Y. Borg, H. C. Heard, Mechanical twinning and slip in experimentally deformed plagioclases. *Contrib. Mineral. Petrol.* **23**, 128–135 (1969).
29. R. C. Pond, "Line defects in interfaces" in *Dislocations in Solids*, F. R. N. Nabarro, Ed. (Elsevier, 1989), vol. **8**, pp. 5–66.
30. P. M. Anderson, J. P. Hirth, J. Lothe, *Theory of Dislocations* (Cambridge University Press, Cambridge, ed. 3, 2017).
31. M. Gong, J. P. Hirth, Y. Liu, Y. Shen, J. Wang, Interface structures and twinning mechanisms of twins in hcp metals. *Mater. Res. Lett.* **5**, 449–464 (2017).
32. T. Hahn, H. Klapper, "Twinning of crystals" in *International Tables for Crystallography. Volume D*, A. Authier, Ed. (Springer, Netherlands, 2006), pp. 393–448.
33. K. M. Knowles, A high-resolution electron microscope study of nickel-titanium martensite. *Philos. Mag. A Phys. Condens. Matter Defects Mech. Prop.* **45**, 357–370 (1982).
34. K. M. Knowles, C. N. F. Ramsey, Type II twinning in devitrite. *Philos. Mag. Lett.* **92**, 38–48 (2012).
35. V. Kahlenberg, D. Girter, E. Arroyaba, R. Kaingl, Devitrite: Structural, spectroscopic, and computer investigations on a crystalline impurity phase in industrial soda lime glass. *Mineral. Petrol.* **100**, 1–9 (2010).
36. D. M. M. Guyoncourt, A. G. Crocker, The deformation twinning mode of crystalline mercury. *Acta Metall.* **16**, 529–534 (1968).
37. J. Wang, I. J. Beyerlein, J. P. Hirth, C. N. Tomé, Twinning dislocations on $\{\bar{1}011\}$ and $\{\bar{1}013\}$ planes in hcp crystals. *Acta Mater.* **59**, 3990–4001 (2011).
38. J. P. Hirth, R. C. Pond, Steps, dislocations and disconnections as interface defects relating to structure and phase transformations. *Acta Mater.* **44**, 4749–4763 (1996).
39. D. Li, R. H. Wagoner, The nature of yielding and anelasticity in metals. *Acta Mater.* **206**, 116625 (2021).
40. G. Proust, C. N. Tomé, A. Jain, S. R. Agnew, Modeling the effect of twinning and detwinning during strain-path changes of Mg alloy AZ31. *Int. J. Plast.* **25**, 861–880 (2009).
41. H. Wang, P. Wu, J. Wang, Numerical assessment of the role of slip and twinning in magnesium alloy AZ31B during loading path reversal. *Metall. Mater. Trans., A Phys. Metall. Mater. Sci.* **46A**, 3079–3082 (2015).
42. R. C. Pond, D. S. Vlachavas, Bicrystallography. *Proc. R. Soc. Lond.* **386A**, 95–103 (1983).